This document contains the draft version of the following paper:

N. Pappafotis, W. Bejgerowski, R. Gullapalli, J.M. Simard, S.K. Gupta, and J.P. Desai. Towards design and fabrication of a miniature MRI-compatible robot for applications in neurosurgery. *ASME Mechanisms and Robotics Conference*, Brooklyn, NY, August 2008.

Readers are encouraged to get the official version from the journal's web site or by contacting Dr. S.K. Gupta (skgupta@umd.edu).

TOWARDS DESIGN AND FABRICATION OF A MINIATURE MRI-COMPATIBLE ROBOT FOR APPLICATIONS IN NEUROSURGERY

Nicholas Pappafotis
Department of Mechanical Engineering
University of Maryland
College Park, MD 20742, USA

Wojciech Bejgerowski
Manufacturing Automation Laboratory
Department of Mechanical Engineering
University of Maryland
College Park, MD 20742, USA

Rao Gullapalli
University of Maryland School of Medicine
Baltimore, MD, USA

J. Marc Simard
University of Maryland School of Medicine
Baltimore, MD, USA

Satyandra K. Gupta
Manufacturing Automation Laboratory
Department of Mechanical Engineering and
The Institute for Systems Research
University of Maryland
College Park, MD 20742, USA

Jaydev P. Desai*
Robotics, Automation, Manipulation, and Sensing (RAMS) Laboratory
Department of Mechanical Engineering
University of Maryland
College Park, MD 20742, USA

ABSTRACT

Brain tumors are among the most feared complications of cancer and they occur in 20–40% of adult cancer patients. Despite numerous advances in treatment, the prognosis for these patients is poor, with a median survival of 4–8 months. The primary reasons for poor survival rate are the lack of good continuous imaging modality for intraoperative intracranial procedures and the inability to remove the complete tumor tissue due to its placement in the brain and the corresponding space constraints to reach it. Intraoperative magnetic resonance imaging (MRI) supplements the surgeon's visual and tactile senses in a way that no other imaging device can achieve resulting in less trauma to surrounding healthy brain tissue during surgery. To minimize the trauma to surrounding healthy brain tissue, it would be beneficial to operate through a narrow surgical corridor dissected by the neurosurgeon. Facilitating tumor removal by accessing regions outside the direct "line-of-sight" of the neurosurgical corridor will require a highly dexterous, small cross section, and MRI-compatible robot. Developing such a robot is extremely challenging task. In this paper we report a preliminary design of 6-DOF robot for possible application in neurosurgery. The robot actuators and body parts are constructed from MRI compatible materials. The current prototype is 0.36" in diameter and weighs only 0.0289 N (2.95 grams). The device was actuated using Flexinol® which is a shape memory alloy manufactured by Dynalloy, Inc. The end-effector forces ranged from 12 mN to 50 mN depending on the robot configuration. The end-effector force to robot weight ratio varied from 0.41 to 1.73. During trials the robot motion was repeatable and the range of motion of the robot was about 90 degrees for the end-effector when one side shape memory alloy (SMA) channel was actuated. The actuation time from the start to finish was about 2.5 s.

1 INTRODUCTION

Brain tumors are among the most feared complications of cancer. Whether a primary (intrinsic) malignancy, or a secondary (metastatic) malignancy, involvement of the brain in a cancer patient is devastating, because it threatens the very personality and identity of the individual, and is invariably the most likely of all complications to directly and severely affect the quality of life. Brain tumors occur in 20–40% of adult cancer patients and despite numerous advances in treatment, the prognosis for these patients is poor, with a median survival of 4–8 months [1].

Currently, the optimal treatment for most brain tumors involves primary surgical resection [1] to remove as much tumor as possible in order to facilitate adjuvant therapies such as radiation and chemotherapy. Despite the lack of class I evidence, it is widely agreed that surgery can improve the functional and vital prognosis when the resection is subtotal or better [2, 3]. The adage remains true that the smaller the "tumor burden", the more likely it is that adjuvant therapies will be beneficial.

* Corresponding author, Phone: (301) 405-4427, Fax: (301) 314-9477, Email: jaydev@umd.edu

Unfortunately, many patients cannot undergo primary surgical resection of their brain tumor and therefore are destined to a poor outcome and premature demise. Reasons vary, but the two most important ones include an unfavorable location of the lesion, usual deep or otherwise inaccessible to conventional neurosurgical techniques, and poor general health of the patient, often seen with metastatic disease, that places the patient at an undue risk for complications from complex brain surgery and general endotrachial anesthesia.

Intraoperative magnetic resonance imaging (MRI) has enjoyed increasing use in academic neurosurgical centers [4, 5, 6]. Its importance rests on the fact that it is often difficult or impossible for even the most experienced neurosurgeon to accurately distinguish tumor from viable brain based on appearance, texture or feel of the tissues. Intraoperative MRI supplements the surgeon's visual and tactile senses in a way that no other imaging device can achieve. In many ways, intraoperative MRI has revolutionized the ability of the neurosurgeon to obtain complete tumor resection without jeopardizing normal tissues [7, 8, 9, 10, 11] with early evidence suggesting that its use is associated with improved survival [3]. Other imaging modalities such as computed tomography (CT) and ultrasound (US) are not feasible since CT leads to radiation exposure and not as good image quality compared to MRI [12].

For intraoperative MRI, the operating room must be specially constructed with appropriate shielding to reduce radiofrequency noise. More constraining is that all surgical instrumentation including electrocautery, fiberoptic headlamp, power drill, ultrasonic aspirator, etcetera, must be entirely MRI-compatible, with only a few items with limited ferromagnetism being used inside of the magnetic field and only with strict precautions [13]. Most constraining of all is that the bore of high field strength magnets is generally too small to allow a human operator the space needed to perform neurosurgery.

Over the past decade or two, research in new surgical techniques has turned to the field of robotics for less invasive and more accurate procedures. The use of multiple degree of freedom telerobotic devices and haptic interfaces such as the MR guided robotic assistant developed by Koseki et al. [14] has revolutionized the speed and accuracy of many surgical procedures by providing the surgeon with unparalleled control of the surgical instruments while at the same time requiring much smaller incisions from which to work through [15].

Today in medicine, most neurosurgeons specialize in a certain region of the brain or on certain disorders of the brain. Procedures are generally disorder specific, in that, only certain disorders in certain areas of the brain have even a chance for operational success. Endoscopic surgery as a minimally invasive technique has been used successfully in certain specific operations such as Craniopharyngioma [16], which is a type of cancer most commonly found in children [16]. However, children have a unique ability to regenerate or reincorporate brain tissue, and this type of noninvasive endoscopic surgery is not often performed in adults because of the possible damage to posterior regions [17]. Operations on adults also generally involve a significant craniotomy, where large amounts of skull must be removed in order to access sites of the brain [16]. This type of invasive surgery is only successful under certain special circumstances and mostly revolves around the easily accessible regions of the brain. Recently some minimally invasive techniques have been tried through the introduction of surgical instruments through the nasal cavity, or beneath the ear [18]. Through the use of these "access points" tumors such as those commonly found in adult pituitary glands can be relatively easily removed bit by bit and with minimal residual morbidity [18]. It is clear, that while promising progress has been made in the field of neurosurgery, we are far from a complete minimally invasive solution for brain surgery applications.

In the field of minimally invasive surgical devices, several important designs have come to fruition such as the MRI compatible 6-DOF liver surgery manipulator constructed by Kim and Kobayashi et al. [19], which demonstrates the possibility of real time MRI surgery using teleoperated robotic devices. The hyper redundant nature of this robot is also explained in detail and is a proven asset in the realm of surgical robotics due to the complexity and skill required by the surgeon [19]. Other devices such as the Light Puncture Robot developed by Taliant et al. [20] have demonstrated similar capabilities using less degrees of freedom, but have only been demonstrated useful on less critical areas of the body, and are therefore not precise enough for brain surgery applications. Brain surgery lags behind most of the fields in surgical robotics because of the unique challenges that the brain and MRI environment pose together. Significant strides have been made toward a complete solution for brain surgery applications, such as the MINERVA project in Switzerland [21], the Robot Assisted Micro Surgical System (RAMS) and the Steady Hand developed by NASA [21]. However, they mostly perform only stereotactic [22] procedures that are inherently not real time MRI active [21]. Despite these significant developments, more research and development on neurosurgical robotics is required before a complete solution to the problem can be attained.

Finding a suitable actuator given the above MRI limitation is also challenging. Typically, well characterized actuators such as electromagnetic motors are not feasible in this application due to the fact that they are fabricated from ferromagnetic materials and permanent magnet parts [23]. Several other actuation methods exist, such as electroactive polymers, electrostatic actuators, piezoelectrics, electrorheological fluids, Lorentz force actuators, cable/rod transmission, pneumatics, and hydraulics. However, most of these are immediately eliminated due to the special requirements in the MRI environment; namely any type of ferromagnetic based actuator or rheologic fluid would disturb the magnetic fields within the MRI and ruin the images. Due to significantly narrow surgical corridor required of the robotic device for minimal damage to the brain tissue (typically 0.35" in diameter), pneumatics and hydraulics are also not feasible. Most importantly, the current state of technology in pneumatics and hydraulics does not lend

itself willingly to use in such a small working volume [24], not to mention that the working fluid of these actuators could be potentially dangerous, if accidentally released inside the brain. Limited cross section area restricts the degrees of freedom to be realized by cable-based drive systems in this application. We are interested in developing a highly dexterous robot with small cross section. Hence, we ruled out a cable-based drive systems with external actuators.

Next, we decided to evaluate shape memory alloy (SMA) based actuators. We began by identifying challenges in SMA-based actuation in the context of our application. We identified the following three challenges in our application. First, the current in SMA wires during actuation may interfere with MRI imaging. We believe that this can be addressed by suppressing the MRI imaging when the robot is being actuated. So the robot will first be actuated and when the robot comes to rest, the imaging will be performed (i.e. imaging and actuation will be performed in a sequential manner). The second challenge is the slow speed of SMA-based actuation. We believe that this application does not require very fast speed. Hence, this should not pose any problem. The final challenge is that the heating of SMA wires may cause damage to the surrounding tissue. We believe that this problem can be solved by incorporating a cooling line. In summary, we concluded that challenges associated with SMA-based actuation were not insurmountable. Hence, we decided to use Flexinol® SMA wires manufactured by Dynalloy, Inc. as a starting point in our prototype development.

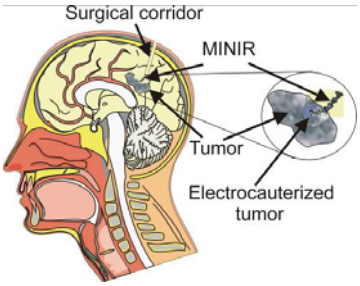

Figure 1. Schematic of the Envisioned Minimally Invasive Neurosurgical Intracranial Robot (MINIR).

To overcome the above limitations in working in an intraoperative MRI environment, we envision developing a Minimally Invasive Neurosurgical Intracranial Robot (MINIR), which would be inserted through a surgical corridor carefully dissected by the neurosurgeon with about 0.35" in diameter. Figure 1 shows a schematic of the envisioned system electrocauterizing the tumor. We envision MINIR to be under the direct control of a human operator, with targeting information obtained exclusively from frequently-updated MRI. Due to the high degrees of freedom of MINIR, it should be able to work outside of the "line-of-site" of the entry trajectory. Like any human neurosurgeon currently, MINIR will resect tumor by positioning an instrument that liquefies tissue and washes out the debris. MINIR will be fully MRI compatible, so that frequently-updated MRI can be used to provide virtual visualization of the target by the human operator as the target's 3-dimensional shape changes during resection. Consequently, the goal of this paper is to develop the first prototype of MINIR with demonstrated degrees of freedom, MRI compatible actuation technology, and MRI compatible robot body.

The rest of the paper is divided as follows. In Section 2 we describe the materials and methods used to design and fabricate the robot. In Section 3 we present the results from our experiments including testing MRI compatibility of the various components, end-effector force measurement, repeatability, and workspace of the robot. Finally, in Section 4 we make conclusions and indicate our future research in this area.

2 MATERIALS AND METHODS

2.1. Design and Fabrication of a 6-DOF Robot

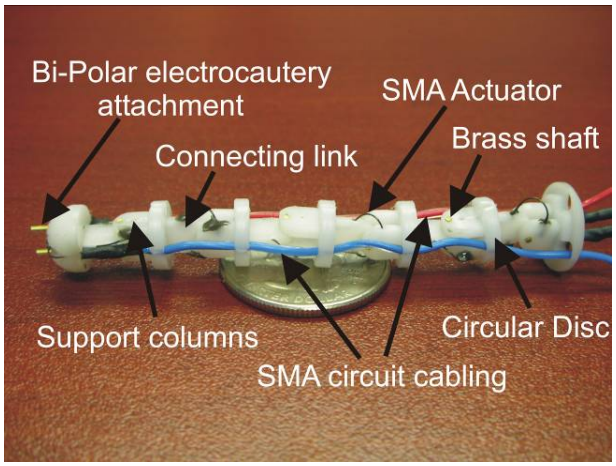

Figure 2. 6-DOF robot with the various components

We have designed and fabricated a 6-DOF robot for applications in minimally invasive intracranial neurosurgery. The fabricated robot is about 0.0289 N in weight (2.95 grams), 2.9375" in length, 0.36" in diameter, and is shown in Figure 2. The robot consists of six revolute joints resulting in six degrees of freedom, and the joints are actuated by 0.012" diameter shape memory alloy, Flexinol® (manufactured by Dynalloy, Inc). Each link is comprised of four primary components: a) circular base disc, b) two supporting columns, and c) connecting link as shown in Figure 2. Each circular base disc is a 0.36" in diameter, with the exception of the first one. Four holes of 0.06" in diameter are milled through the discs to allow for the passage of electrical wiring from the tip of the robot to the base, needed to actuate the individual SMA circuit. Two additional holes have been milled in each circular base to allow for the electrocautery wire to pass through to reach the two probe tips. The first base disc is 0.5" diameter to allow for holding the robot during testing.

However, in practice, it can be also made to be 0.36" in diameter without any consequence. In this prototype we have not developed the bipolar electrocautery system since our primary goal was to develop the actuation mechanism and choose the robot components that would not cause any artifact in the MRI image. The two side support columns were milled with a 0.03125" diameter hole at the right angles to allow for the passage of the SMA wire. The fourth component of the link was the "connecting link" with 0.03425" diameter hole to allow for the brass shaft to pass through with sufficient hole clearance to create a revolute joint. Six of such individual links were connected with the last link having a hemispherical cap for attachment of the bi-polar electrocautery probe tips as represented in Figure 2.

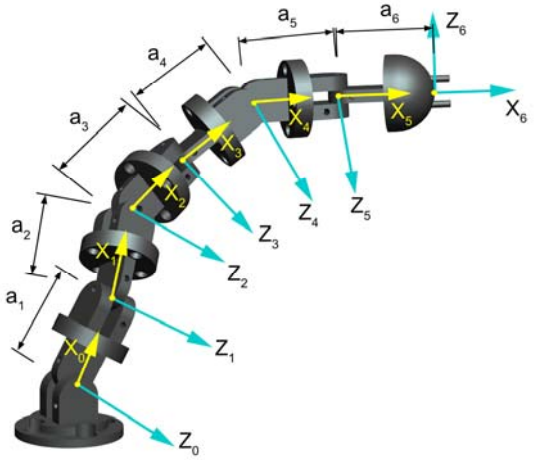

Figure 3. Schematic of the 6-DOF Robot with Reference Frames.

The kinematic structure of the entire mechanism is shown in Figure 3 along with the joint axes labeled. Based on the frame assignment for the various joints, the D-H parameters for the robot are given in Table 1.

Table 1: D–H Parameters.

Axis (Joint) i	a_i	d_i	α_i	θ_i
1	a_1=0.43"	0	90°	θ_1
2	a_2=0.43"	0	-90°	θ_2
3	a_3=0.43"	0	90°	θ_3
4	a_4=0.43"	0	-90°	θ_4
5	a_5=0.43"	0	90°	θ_5
6	a_6=0.43"	0	-90°	θ_6

where a_i is the link length, d_i is the joint offset, α_i is the twist angle, and θ_i is the joint angle rotation. Based on the above parameters we can compute the rotation matrix, R_5^0, and the displacement vector, d_5^0, representing the displacement of the point on the end-effector with respect to the fixed base frame. We define U_i and V_i as 3x3 matrices given by:

$$U_i = \begin{bmatrix} \cos\theta_i & -\sin\theta_i & 0 \\ \sin\theta_i & \cos\theta_i & 0 \\ 0 & 0 & 1 \end{bmatrix} \quad V_i = \begin{bmatrix} 1 & 0 & 0 \\ 0 & \cos\alpha_i & -\sin\alpha_i \\ 0 & \sin\alpha_i & \cos\alpha_i \end{bmatrix} \tag{1}$$

and S_i as 3x1 vector given by:

$$S_i = \begin{bmatrix} a_i \\ 0 \\ d_i \end{bmatrix} \tag{2}$$

Based on this representation, the rotation matrix R_6^0 and the displacement vector d_6^0 are given by:

$$R_6^0 = U_1V_1U_2V_2U_3V_3U_4V_4U_5V_5U_6V_6 \tag{3}$$

$$d_6^0 = U_1S_1 + U_1V_1U_2S_2 + U_1V_1U_2V_2U_3S_3 + U_1V_1U_2V_2U_3V_3U_4S_4 + U_1V_1U_2V_2U_3V_3U_4V_4U_5S_5 + U_1V_1U_2V_2U_3V_3U_4V_4U_5V_5U_6S_6 \tag{4}$$

Due to space constraints, the symbolic expression for the above equations has not been presented.

2.2. Robot Fabrication

The body of the device is made from acetal resin engineering plastic known as Delrin® (3M) which is completely MR compatible, as shown in MR images in Figure 7. The fabrication of the robot links is done by machining 0.125" and 0.25" thick Delrin® sheets, followed by manual clean-up and assembly of the parts. Particular parts of the link are modeled in ProEngineer WildFire 3.0 software, which also allows for creation of the machining NC-sequence. The machine used to manufacture the parts is BenchmanXT CNC-machine. The machine positioning accuracy is ± 0.0002" (0.00508 mm). Benchman XT 2.0 software is used to control the CNC-milling machine and to verify CNC programs.

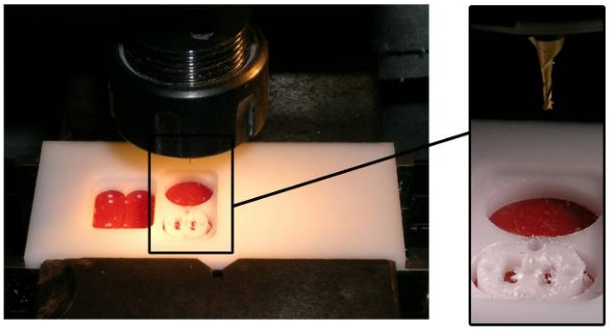

Figure 4. Machining Setup for Robot Linkages.

The machining setup is shown in Figure 4. The raw material is pre-cut to 1.5"x3.0" pieces and clamped on the machine table. The appropriate tools are assigned proper z-axis offsets. Then the NC-sequence is executed. The machining operations include hole making with 0.03125" drill bit, volume milling and profiling with 0.1875" end-mill, pocketing and profiling with 0.03125" end-mill and surface milling with 0.0625" ball-end mill. After CNC-machining, the parts are manually cleaned from the machining flesh with a Xacto knife. The SMA channels inside the parts are then manually drilled on the same machine, using multiple part setups in the clamp. The

holes in the rotating parts are also re-drilled with 0.0345" drill bit to obtain the right clearance for the shaft. The schematic of all the four components of a link, namely, circular base disc, two supporting columns, and connecting link are shown in Figure 5.

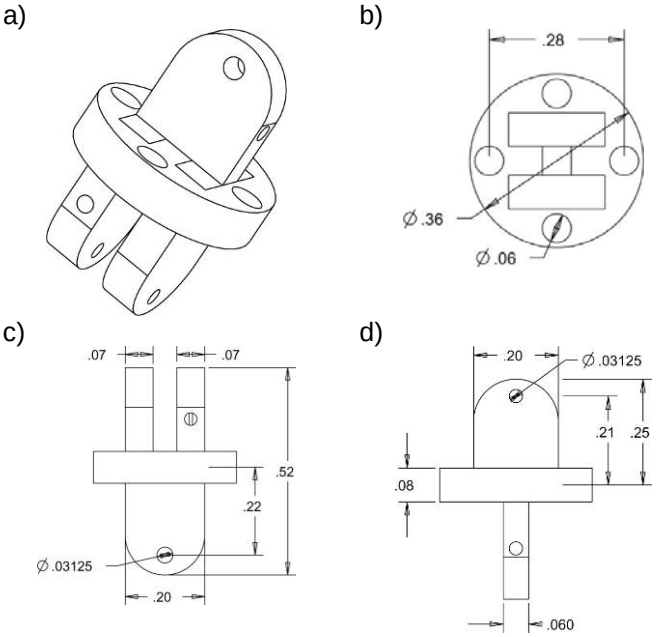

Figure 5. a) Isometric View of each Link, b) Circular Base Disc, c) and d) Views showing the Two Supporting Columns and Connecting Link to Show the Path for SMA Wire as well as the Brass Shaft.

For now the assembly of the robot is facilitated by tight tolerances (snapping pieces together) and then the use of an adhesive such as 5 minute epoxy. Once assembled, the entire device is a 6-DOF robot arm as shown in Figure 1.

2.3. SMA Actuation

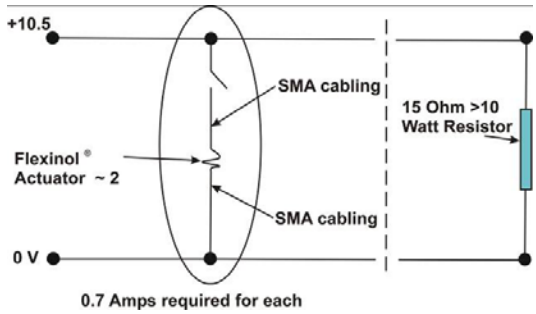

Figure 6. Open-loop Control Circuit for Robot.

The current control system of the robot is an open loop switching unit. A schematic of the circuit is shown in Figure 6. Each of the switches on this unit has the capability of controlling a SMA actuator. Each SMA actuator is incorporated into a circuit and current is run through this circuit. The current heats the SMA due to its resistance, resulting in the temperature rise of the SMA above its austenitic transition temperature and flexing back into its straight position. The joints actuate as long as the current is passing through the SMA on each side as shown in Figure 6. Once the temperature of the SMA falls back below the transition temperature, it is no longer actuated. The spring force of the opposing SMA actuator will return the joint to its zero position. In the first prototype, there are only two complete SMA circuits. Therefore actuation occurs in one or the other directions. In the future it may be desirable to develop an individual actuation for each joint of the robot as well as improved cooling strategies to control each link motion better. These requirements may call for some microfabrication processing.

3 RESULTS

3.1. MRI Imaging

We took several images of the various components of the robot in MRI. Figure 7(a) shows the image of the end-effector with the bi-polar electrocautery attachment of two brass probes.

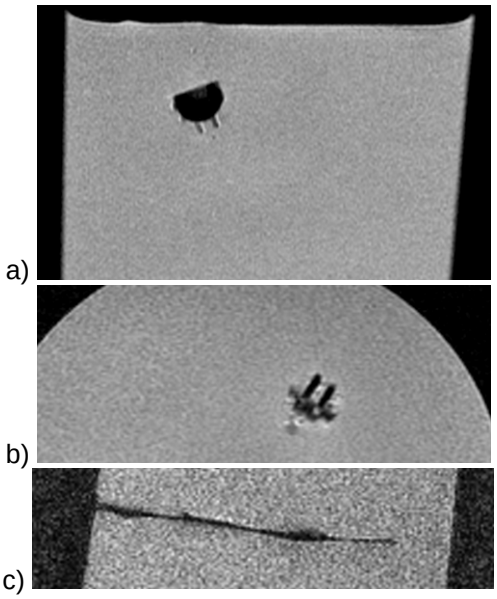

Figure 7. MRI Images of the Individual Components of the Robot: a) End-effector with Two Probes for Bi-polar Electrocautery Setup, b) Individual Link Showing the Circular Disc as well as the Two Support Columns with a Brass Shaft, and c) the SMA Wire

As seen in Figure 7, there are no artifacts introduced by brass as well as Delrin® in MRI. Figure 7(b) shows the image of the circular base disc with the two supporting columns as well as the brass shaft. Here also no artifacts are produced. Finally, in Figure 7(c), we imaged the Flexinol® actuator and the MRI image is very clear without any artifact. To quantify the induced disturbance to the images, we obtained the signal-to-noise ratio (SNR) of the images, where SNR is defined as

the ratio of the mean pixel value of the signal and the standard deviation of the pixel value of the background noise [25]. The SNR was observed to be 40.0361 for Figure 7(a) and 16.9295 for Figure 7(b), which indicates that the image features were sharply identifiable in MRI. As an example, we also took images of other materials, such as 0.125"-diameter 400 series stainless steel bearings, which we initially planned to use in the prototype. As seen in Figure 8(a), there is significant distortion in the image and a 0.125" diameter bearing produces a black field of about 1" in diameter. Additionally, Figure 8(b) shows the image of a magnetically neutral material but with significant artifact due to the presence of a dipole in the image.

a) 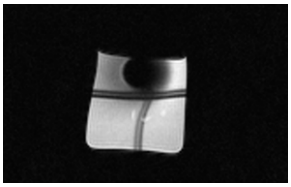 b) 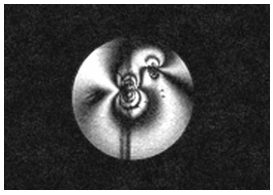

Figure 8. Magnetically Neutral Materials Producing Significant Artifacts in the Image: a) 400 Series Stainless Steel Bearing of 0.125" outer Diameter Produces about 1" Diameter Distortion in the Image and b) Magnetically Neutral Material Showing the Presence of Dipole and Image Artifacts under MRI.

3.2. Motion Repeatability

Figure 9(a) shows the initial position of the device on the grid while Figure 9(b) shows the image of the device when fully actuated along one SMA cabling side. As pictured in Figure 9, there is approximately a 90 degree range of motion of the end-effector. We performed experiments to see if this motion was repeatable and we found that the motion was repeatable to within a few millimeters. Once we develop a control methodology for SMA actuation, we expect this to improve. Additionally, we also measured the time to actuate from the initial configuration to the final configuration. This was measured to be 2.5 s.

a) 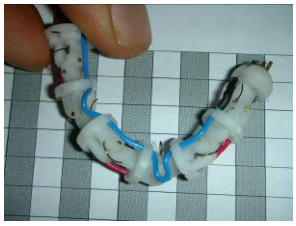 b) 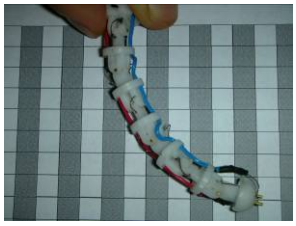

Figure 9. a) Initial Position of the Robot and b) Final Position of the Robot During the Full Range of Actuation of One Side of the SMA Circuit.

3.3. End-Effector Forces

Figure 10. End-Effector Force Measurement using a GSO-10 Load Cell

To measure the end-effector force during actuation, we contacted the end-effector probe tip to the force sensor as shown in Figure 10. We used a load cell (Transducer Technology Inc., Model: GSO-10) with maximum measurement range of 98.1 mN and accuracy of 50 μN. The end-effector force when all links were at zero-angle configuration and actuated is plotted in Figure 11 and it is on an average about 12 mN. When the robot was bent at a larger angle and actuated, the end-effector force was significantly higher, at around 50 mN, as shown in Figure 12. Considering the weight of the robot of about 0.0289 N, the end-effector force to weight ratio varies from 0.41 to 1.73 for the two force profiles shown in Figures 11 and 12, which is a significant amount.

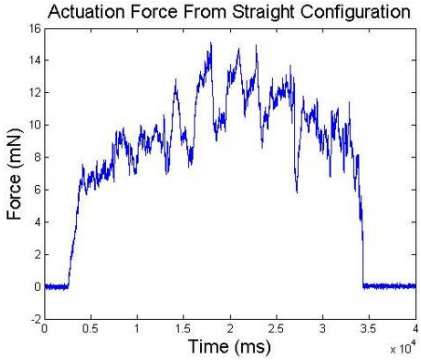

Figure 11. End-effector Force when the Robot is Actuated from the Nominal Zero Degree Configuration.

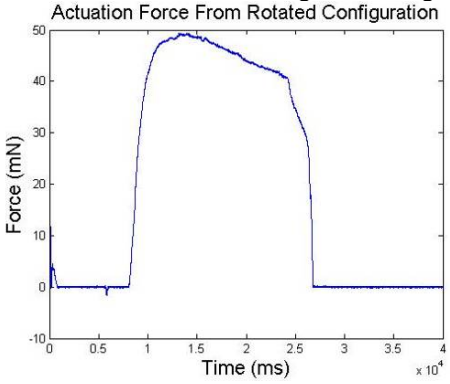

Figure 12. End-effector Force when the Robot is Bent around and then Actuated.

4 CONCLUSIONS AND FUTURE WORK

We have developed a preliminary design of a miniature 6-DOF robot for possible application in neurosurgery. The entire robot is constructed from MRI compatible actuators and body parts. The current prototype is 0.36" in diameter and weighs 2.94 grams.

The device was actuated using Flexinol® which is a shape memory alloy manufactured by Dynalloy, Inc. The end-effector forces ranged from 12 mN to 50 mN, depending on the robot configuration. During trials the robot motion was repeatable and the range of motion of the robot was about 90 degrees for the end-effector when one side SMA channel was actuated. The actuation time from the start to finish was about 2.5 s. MRI imaging of the various components of the robot showed that they were MRI compatible and there appeared to be no artifacts in the image.

Future work will require significant improvements in the design as well as individual actuation of the joints, if necessary. We envision using a dedicated cooling line for each joint to achieve selective joint motion. Cooling can be achieved by using liquid nitrogen or liquid carbon dioxide. We would also need to be able to track the tip of the robot in MRI using MRI visible markers. Additional markers at other locations on the robot would also need to be tracked, if necessary, to provide better visualization of the robot in the MRI image. Additionally, implementation of bi-polar electrocautery, removal of electrocauterized material through suction, and various other actuation technologies would need to be investigated. We also envision using a remote teleoperative system to guide the end-effector within the magnet and feel the end-point and tissue interaction forces. This can be achieved by, for example, calibrating the input current to the SMA actuation force at the end-point. Further analysis of the hysteresis of the SMA based actuation as well as heat loss calculation will help to improve the control bandwidth. To enable a more compact design and electronic circuitry for individual joint actuation, a completely dedicated control board using some of the same principles listed in the control section above will be constructed and an embedded microcontroller will be programmed to control this via a software interface. Additionally, it would also require microfabrication techniques to develop an individual actuator for each joint, if necessary. While there are significant challenges ahead, the work presented in this paper is the first attempt towards the development of the envisioned MINIR system outlined in the introduction.

ACKNOWLEDGMENTS

We acknowledge the internal support of University of Maryland, College Park, to perform some of this work. Part of this research has also been supported by the NSF grants DMI-0457058 and OCI-0636164. Opinions expressed in this paper are those of the authors and do not necessarily reflect opinions of the sponsors.

REFERENCES

[1] Siker, M. L. and Mehta, M. P., 2007, "Resection versus Radiosurgery for Patients with Brain Metastases", *Future Oncol,* Vol. **3** (1), pp. 95-102.

[2] Mandonnet, E., Jbabdi, S., Taillandier, L., Galanaud, D., Benali, H., Capelle, L. and Duffau, H., 2007, "Preoperative Estimation of Residual Volume for WHO Grade II Glioma Resected with Intraoperative Functional Mapping" *Neuro Oncol,* Vol. **9** (1), pp. 63-69.

[3] Claus, E. B., Horlacher, A., Hsu, L., Schwartz, R. B., Dello-Iacono, D., Talos, F., Jolesz, F. A. and Black, P. M., 2005, "Survival Rates in Patients with Low-Grade Glioma after Intraoperative Magnetic Resonance Image Guidance", *Cancer*, Vol. **103** (6), pp. 1227-1233.

[4] Nimsky, C., Ganslandt, O., von Keller, B. and Fahlbusch, R., 2006, "Intraoperative High-Field MRI: Anatomical and Functional Imaging", *Acta Neurochirurgica Supplements*, Vol. **98**, pp. 87-95.

[5] Busse, H., Schmitgen, A., Trantakis, C., Schober, R., Kahn, T. and Moche, M., 2006, "Advanced Approach for Intraoperative MRI Guidance and Potential Benefit for Neurosurgical Applications" *J Magn Reson Imaging*, Vol. **24** (1), pp. 140-151.

[6] Schulder, M., Salas, S., Brimacombe, M., Fine, P., Catrambone, J., Maniker, A. H. and Carmel, P. W., 2006, "Cranial Surgery with an Expanded Compact Intraoperative Magnetic Resonance Imager. Technical note", *J Neurosurg*, Vol. **104** (4), pp. 611-617.

[7] Muragaki, Y., Iseki, H., Maruyama, T., Kawamata, T., Yamane, F., Nakamura, R., Kubo, O., Takakura, K. and Hori, T., 2006, "Usefulness of Intraoperative Magnetic Resonance Imaging for Glioma Surgery", *Acta Neurochir Suppl*, Vol. **98**, pp. 67-75.

[8] Nimsky, C., von Keller, B., Ganslandt, O. and Fahlbusch, R., 2006, "Intraoperative High-Field Magnetic Resonance Imaging in Transsphenoidal Surgery of Hormonally Inactive Pituitary Macroadenomas", *Neurosurgery*, Vol. **59** (1), pp. 105-114.

[9] Nimsky, C., Ganslandt, O., Buchfelder, M. and Fahlbusch, R., 2006, "Intraoperative Visualization for Resection of Gliomas: the Role of Functional Neuronavigation and Intraoperative 1.5 T MRI", *Neurol Res*, Vol. **28** (5), pp. 482-487.

[10] Iseki, H., Muragaki, Y., Nakamura, R., Ozawa, N., Taniguchi, H., Hori, T. and Takakura, K., 2005, "Intelligent Operating Theater using Intraoperative Open-MRI", *Magn Reson Med Sci*, Vol. **4** (3), pp. 129-136.

[11] Oh, D. S. and Black, P. M., 2005, "A Low-Field Intraoperative MRI System for Glioma Surgery: is it Worthwhile?", *Neurosurg Clin N Am*, Vol. **16** (1), pp. 135-141.

[12] Stoianovici, D., 2005, "Multi-Imager Compatible Actuation Principles in Surgical Robotics", *Int J Medical Robotics and Computer Assisted Surgery*, Vol. **1** (2), pp. 86-100.

[13] Hall, W. A., Galicich, W., Bergman, T. and Truwit, C. L., 2006, "3-Tesla Intraoperative MR Imaging for Neurosurgery", *J Neurooncol*, Vol. **77** (3), pp. 297-303.

[14] Koseki, Y., Chinzei, K., Koyachi, N. and Arai, T., 2000, "Robotic Assist for MR-Guided Surgery Using Leverage and Parallelepiped Mechanism", *Lecture Notes in Computer Science 1935*, pp. 940-948.

[15] Zemiti, N. and Morel, G., 2007, "Mechatronic Design of a New Robot for Force Control in Minimally Invasive Surgery", *ASME Transactions on Mechatronics*, Vol. **12** (2), pp. 143-153.

[16] "Functional Neurosurgery – Center for Minimally Invasive Neurosurgery", 2005, http://www.neuroendoscopy.info/functionalNeurosurgery.asp.

[17] Johnson, D. and Wu, S., 1995, "Foundations of Cellular Neurophysiology", *The MIT Press, Cambridge, MA*, pp. 1-183.

[18] Bails, J., 2005, "Pittsburgh Doctors Pioneer Technique for Brain Surgery," *Pittsburgh Tribune - Review*, http://www.pittsburghlive.com/x/pittsburghtrib/s_371456.html.

[19] Kim, D., Kobayashi, E., Dohi, T. and Sakuma, I., 2002, "New, Compact MR-Compatible Surgical Manipulator for Minimally Invasive Liver Surgery", *Lecture Notes in Computer Science 2488*, pp. 99-106.

[20] Taillant, E., Avila-Vilchis, J., Allegrini, C., Bricault, I. and Cinquin, P., 2004, "CT and MR Compatible Light Puncture Robot: Architectural Design and First Experiments", *Lecture Notes in Computer Science 3217*, pp. 145-152.

[21] McBeth, P. B., Louw, D. F., Rizun, P. R. and Sutherland, G. R., 2004, "Robotics in Neurosurgery", *The American Journal of Surgery*, Vol. **188** (4), pp. 68-75.

[22] Burckhardt, C. W., Fluty, P. and Glauser, D., 1995, "Stereotactic Brain Surgery", *IEEE Engineering in Medicine and Biology*, Vol. 14 (3), pp. 314-317.

[23] Gassert, R., Yamamoto, A., Chapuis, D., Dovat, L., Bleuler, H. and Burdet, E., 2006, "Actuation Methods for Applications in MR Environments", *Concepts in Magnetic Resonance Part B (Magnetic Resonance Engineering)*, Vol. **29B** (4), pp. 191-209.

[24] Moser, R., Gassed, R., Burdet, E., Sachel, L., Woodtli, H. R., Emi J., Maeder, W. and Bleuler, H., 2003, "An MR Compatible Robot Technology", *International Conference on Robotics and Automation, Taipei, Taiwan*, Vol. **1**, pp. 670-675.

[25] Hidler, J., Hodics, T., Xu, B., Dobkin, B. and Cohen, L., 2006, "MR Compatible Force Sensing System for Real-Time Monitoring of Wrist Moments During MRI Testing," *Journal of Neuroscience Methods*, Vol. **155**, pp. 300-307.

\